

Sensing-Communication-Computing-Control Closed Loop for Unmanned Space Exploration

Xinran Fang, *Student Member, IEEE*, Wei Feng, *Senior Member, IEEE*, Yunfei Chen, *Senior Member, IEEE*, Ning Ge, *Member, IEEE*, and Gan Zheng, *Fellow, IEEE*

Abstract—With a growing interest in outer space, space robots have become a focus of exploration. To coordinate them for unmanned space exploration, we propose to use the “mother-daughter structure”. In this setup, the mother spacecraft orbits the planet, while daughter probes are distributed across the surface. The mother spacecraft senses the environment, computes control commands and distributes them to daughter probes to take actions. They synergistically form sensing-communication-computing-control (SC³) loops. Since the SC³ loop is indivisible, we thereby optimize the spacecraft-probe downlink within SC³ loops to minimize the linear quadratic regulator (LQR) cost. The optimization variables are block length and transmit power. On account of the cycle-time constraint, the spacecraft-probe downlink operates in the finite block length (FBL) regime. To solve the nonlinear mixed-integer problem, we first identify the optimal block length and then transform the power allocation problem into a tractable convex problem. Additionally, we derive the approximate closed-form solutions for the proposed scheme and also for the max-sum rate and max-min rate schemes. On this basis, we reveal their different power allocation principles. Moreover, we find that for time-insensitive control tasks, the proposed scheme demonstrates equivalence to the max-min rate scheme. These findings are verified through simulations.

Index Terms—Linear quadratic regulator (LQR) cost, mother-daughter structure, power allocation, sensing-communication-computing-control (SC³) loop, unmanned space exploration.

I. INTRODUCTION

A. Background and Motivation

Planetary exploration is one of the most important space exploration activities. In recent years, many countries have made substantial progress in planetary exploration. Taking Mars as an example, during the launch window of 2020, China, America and the United Arab Emirates dispatched their spacecrafts to Mars [1]. Subsequently, in 2021, China’s Zhurong rover and America’s Perseverance rover successfully landed on the Martian surface. Throughout its lifetime, the Zhurong rover has returned more than 1000 GB data [2], which provide important clues to figure out the Mar’s evolution and potential habitability.

Despite these exciting results, space exploration still faces numerous challenges. The success rate of Mars exploration is around 50%, while the success rate of landing on the

Martian surface is around 20% [3]. One significant factor is the long transmission latency of deep space communication (DSC). This makes it impossible for the Earth center to provide instructions during the landing process. The lander has to analyze the situation and trigger a series of actions autonomously in a highly uncertain environment, making the landing process a high risk.

To improve the reliability of unmanned space exploration, we propose to use the “mother-daughter structure” to coordinate space robots. Actually, the “mother-daughter structure” is not new in the aerospace field. A typical example is the international space station, which consists of a core module of a spacecraft and various auxiliary modules [4]. The spacecraft can flexibly dock with auxiliary modules to accomplish different missions. In Fig. 1, we present our envisaged “mother-daughter structure” in unmanned space exploration. The central component is a mother spacecraft, which carries a lander that contains multiple daughter probes. At first, they go through a series of flight processes, i.e., launch phase, transfer orbit phase, planet approach phase and enter the planet’s orbit. Then, the mother spacecraft remains in the planet’s orbit. It releases the lander to the target area. Afterward, the daughter probes are distributed to different regions and execute different exploration tasks. Compared with rovers such as the Perseverance, the daughter probes are smaller, lighter, and more cost-effective. This makes it possible to packet and carry more than one probe in a single mission. With this redundancy, the malfunction of some probes would not result in the failure of the whole mission and thus increases the fault tolerance of unmanned space exploration. Moreover, the union of multiple “mother-daughter structures” can lead to a large-scale space exploration system. By employing these interconnected structures, exploration missions can be simultaneously and synchronously conducted across multiple regions, significantly enhancing the efficiency.

To enable these relatively inferior probes to conduct arduous exploration tasks, cooperation between the mother spacecraft and daughter probes is crucial. The mother spacecraft should be powerful and carry various cutting-edge devices, i.e., precise sensors, advanced computing modules and high-gain antenna arrays. If the planetary exploration objective is to acquire a comprehensive understanding of the explored planet, sensing-type probes will take a large portion. They collect data from the planet and upload them to the spacecraft. The spacecraft analyses these data and relays the important information to Earth. For future missions involving sample return and base construction, there will be a greater demand for executing-type

X. Fang, W. Feng, and N. Ge are with the Department of Electronic Engineering, Tsinghua University, Beijing 100084, China (e-mail: fxr20@mails.tsinghua.edu.cn, fengwei@tsinghua.edu.cn, and gening@tsinghua.edu.cn).

Y. Chen is with the Department of Engineering, University of Durham, Durham DH1 3LE, U.K. (e-mail: yunfei.chen@durham.ac.uk).

G. Zheng is with the School of Engineering, University of Warwick, CV4 7AL Coventry, U.K. (e-mail: gan.zheng@warwick.ac.uk).

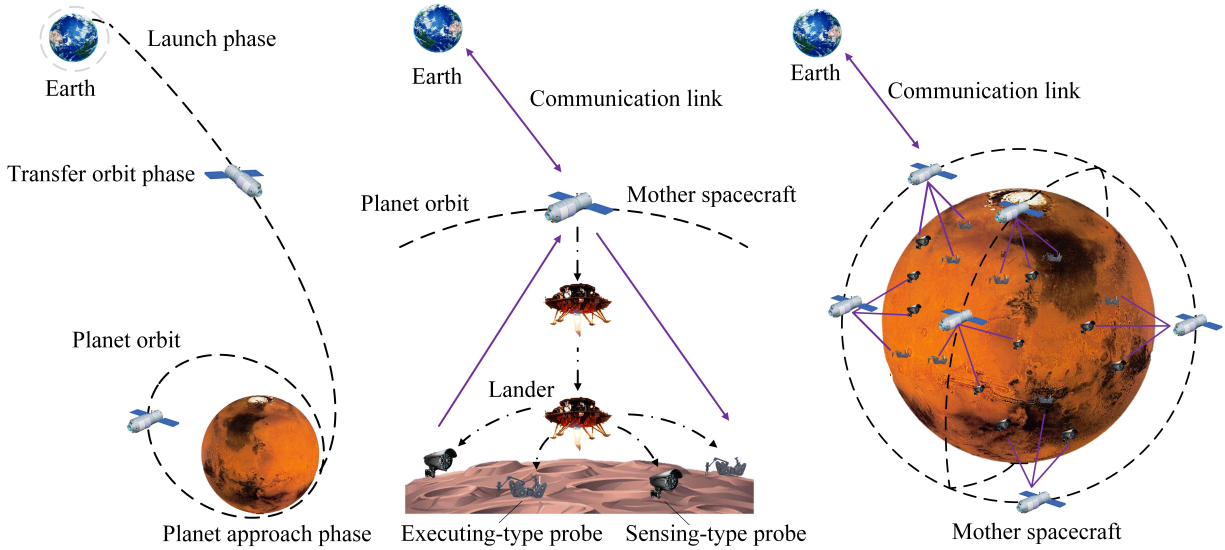


Fig. 1. Illustration of the “mother-daughter structure” in unmanned space exploration.

probes. For these missions, the mother spacecraft assumes the responsibility of sensing the environment, performing analysis, and providing guidance to the executing-type probes. Operating in a cyclical manner, the spacecraft and executing-type probes synergically form sensing-communication-computing-control (SC^3) loops. Relying on the effective feedback mechanism, the SC^3 loop can adapt to the varying environment and finish different control-type tasks.

In this paper, we use the SC^3 loop of the “mother-daughter structure” to finish the control-type task in unmanned space exploration. In the literature, few studies have investigated the SC^3 loop from a systematic perspective. The communication researchers mostly took the communication link as the investigated objective and addressed the communication challenges in deep space. While improving communication performance is crucial for unmanned space exploration, separating the communication process from the SC^3 loop is not the optimal choice. It overlooks the communication impact on the overall functioning of the SC^3 loop. On the other hand, researchers in control have been studying the whole SC^3 loop for a long time. Specifically, in the domain of the networked control system (NCS), where sensors, controllers, and actuators are interconnected via a shared network, it has been observed that communication imperfections can have adverse effects on closed-loop control. Related studies have paid particular attention to unveiling the fundamental relationships between communication and control. Building upon these results, many optimization schemes were proposed to adapt the communication strategies to closed-loop control. In the following, we review related studies of DSC and NCS.

B. Related Works

1) *DSC*: DSC plays an important role in space exploration. It assumes the responsibility of data exchange, telemetry, remote control etc. for various space missions. Due to the long transmission distance between spacecrafts or probes located in

deep space and Earth centers, DSC encounters unique challenges compared with ground-based communication. Many studies have addressed these challenges from different perspectives, including communication protocols, networking, resource optimization etc. For example, Ha *et al.* proposed a reinforcement learning-based link selection strategy to improve the streaming performance of DSC [9]. To tackle the solar scintillation effect, Xu *et al.* proposed a dual-hop mixed communication system, which comprises a radio frequency link between the Earth and the relay satellite and a free space optical link between the satellite and a deep space probe [10]. To address the challenge of intermittent connection, the delay-tolerant network (DTN) has been developed, which uses the store-and-forward strategy to combat the interruption. On this basis, Yang *et al.* proposed a hybrid bundle retransmission scheme to ensure the DTN reliability [11]. Rango *et al.* proposed an adaptive bundle rate scheme to combat the concurrent bundle transmissions [12]. In terms of the network structure, Wan *et al.* proposed a structured solar system satellite relay constellation network and detailed the mathematical model, topology design and performance analysis [13]. These studies made great contributions to improving communication performance of the deep space network, providing a solid foundation for unmanned space exploration.

2) *NCS*: Taking communication imperfections such as delays, dropouts, and rate limitations into account, researchers in control have paid great attention to the relationship between communication and control. For example, under the condition of a limited data rate, Tatikonda *et al.* investigated the minimal data-rate requirement to stabilize the linear time-invariant system [14]. It was proven that only when the data rate exceeds the intrinsic entropy, can the system be stabilized [15]. Afterward, Nair *et al.* extended this result to nonlinear systems. The stable condition was defined by a new concept named topological feedback entropy [16]. Furthermore, Kostina *et al.* generalized these results to vectorial, non-Gaussian, and partially observed systems. By giving the cycle rate, the lower

bound of the linear quadratic regulator (LQR) cost was derived [17]. Afterward, the stable condition was investigated under different communication delay [18]–[20].

Building upon these results, numerous resource optimization schemes have been proposed for NCSs. For example, Lyu *et al.* devised a control-aware cooperative transmission scheme that jointly optimized channel allocation, power control, and relay cooperation [21]. Girgis *et al.* provided a prediction-based control scheme to minimize the age of information and the transmit power under bounded control states [22]. Yang *et al.* developed a framework to optimize a new metric named the energy-to-control efficiency [23]. Lei *et al.* proposed a multi-loop optimization scheme to minimize the sum LQR cost. The transmit power was balanced among different loops [24]. Chang *et al.* co-optimized the bandwidth, transmit power, and control convergence rate to maximize the spectrum efficiency [25]. Esien *et al.* proposed a control-aware scheduling scheme that adapted the data transmission to channel dynamics and system states [26]. While related work took a significant step to adapt data transmissions to the closed-loop control, many of them still took communication metrics as the objective, and the resulting solutions only guaranteed basic control performance.

C. Main Contributions

In this paper, we propose to use the “mother-daughter” structure in unmanned space exploration. The mother spacecraft and daughter probes synergistically form multiple SC^3 loops. Since the SC^3 loop is indivisible, it is necessary to optimize them from a systematic perspective. Focusing on the command transmission in the spacecraft-probe downlink, we consider the communication optimization within SC^3 loops. The main contributions are listed as follows.

- 1) We use the SC^3 loop of the “mother-daughter structure” to execute the control-type task in unmanned space exploration. Since the SC^3 loop is indivisible, we integrate the spacecraft-probe downlink optimization into SC^3 loops. The proposed scheme takes the control metric, namely the LQR cost, as the objective and the transmit power and block length as variables for optimization. Considering the cycle-time constraint, the spacecraft-probe downlink operates in the FBL regime.
- 2) To solve the formed nonlinear integer problem, we first derive the optimal block length based on the monotonicity of the rate-cost objective function. Subsequently, we analyze the monotonicity and concavity-convexity of the achievable rate expression in the FBL regime and the rate-cost function. Building upon these insights, we transform the power allocation problem into a standard convex problem and employ the convex optimization technique to solve it.
- 3) To facilitate practical implementation, we provide approximate closed-form solutions of the transmit power for the proposed scheme, as well as for two communication-oriented schemes: the max-sum rate scheme and the max-min rate scheme. By showing the equivalence between the proposed scheme and the max-min rate scheme for time-insensitive control tasks,

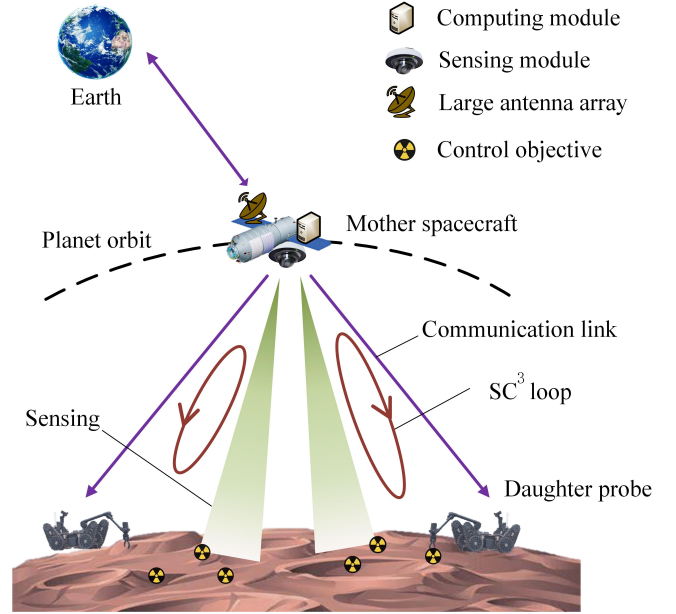


Fig. 2. Illustration of an unmanned space exploration system that comprises a mother spacecraft and multiple daughter probes. The spacecraft and probes synergistically form multiple SC^3 loops and each loop takes charge of a control-type subtask.

we reveal the fairness-minded nature of the proposed scheme.

- 4) In the simulation, we use appropriate parameters to model the near planet environment. Simulation results confirm the effectiveness of the proposed scheme in improving the control performance of the “mother-daughter structure” and also validate our findings.

D. Organization and Notation

The rest of this paper is organized as follows. Section II introduces the “mother-daughter structure” and the SC^3 loop. Section III presents the spacecraft-probe downlink optimization scheme and its solution. Section IV derives the closed-form solution of the proposed scheme and compares it with that of the max-sum rate scheme and max-min rate scheme. Section V presents simulation results. Section VI draws conclusions.

Throughout this paper, vectors and matrices are represented by lower and upper boldface symbols. $\mathbb{R}^{m \times m}$ represents the set of $m \times m$ real matrices, \mathbf{I}_m is the $m \times m$ unit matrix, and $\mathbf{0}_m$ is the $m \times m$ zero matrix. $\lambda(\mathbf{A})$ denotes the eigenvalue of matrix \mathbf{A} .

II. SYSTEM MODEL

As shown in Fig. 2, we consider a “mother-daughter structure” in unmanned space exploration. The mother spacecraft is located in the planet’s orbit and carries advanced sensing, communication and computing modules. In every control cycle, it senses system states, calculates control commands and distributes these commands to daughter probes. The daughter probes then take control actions. Working in a cyclical manner, they synergistically form multiple SC^3 loops. In addition, there

exists a communication link between the spacecraft and Earth. The spacecraft receives telemetry, tracking, and command and sends the collected data back via this link. We assume this “mother-daughter structure” includes K \mathbf{SC}^3 loops. Each \mathbf{SC}^3 loop operates an LQR-based controller to execute a control-type subtask. For the k th \mathbf{SC}^3 loop at time index i , we apply the following state-space equation to characterize the relationship between the system dynamics and the control behavior of the daughter probe

$$\mathbf{x}_{k,i+1} = \mathbf{A}_k \mathbf{x}_{k,i} + \mathbf{B}_k \mathbf{u}_{k,i} + \mathbf{v}_{k,i}, \quad (1)$$

where $\mathbf{x}_{k,i} \in \mathbb{R}^{m \times 1}$ is the system internal state and $\mathbf{u}_{k,i} \in \mathbb{R}^{m \times 1}$ is the control input, which characterizes the impact of the probe behavior on the system state. The matrices $\mathbf{A}_k \in \mathbb{R}^{m \times m}$ and $\mathbf{B}_k \in \mathbb{R}^{m \times m}$ are determined by the system dynamics and $\mathbf{v}_{k,i} \in \mathbb{R}^{m \times 1}$ is the system uncertainty, whose covariance matrix is denoted as $\Sigma_{\mathbf{v}_k} \in \mathbb{R}^{m \times m}$. The system is unstable ($\lambda(\mathbf{A}_k) > 1$) and it can be stabilized using $(\mathbf{A}_k, \mathbf{B}_k)$. In practice, the state-space equation is non-linear. To apply the LQR technique for control design, (1) is obtained by linearizing the system dynamics around the working point. Although simplified, it is still effective to characterize the system’s dynamics and its response to the probe’s control behavior.

Moving forward, in each control cycle, the spacecraft first senses system states. The sensing process is modeled as a partially observed process

$$\mathbf{y}_{k,i} = \mathbf{C}_k \mathbf{x}_{k,i} + \mathbf{w}_{k,i}, \quad (2)$$

where $\mathbf{y}_{k,i} \in \mathbb{R}^{m \times 1}$ is the observation state, $\mathbf{C}_k \in \mathbb{R}^{m \times m}$ is the observation matrix, and $\mathbf{w}_{k,i} \in \mathbb{R}^{m \times 1}$ is the sensing noise, which is assumed to conform to the Gaussian distribution. The covariance matrix of the sensing noise is denoted as $\Sigma_{\mathbf{w}_k} = \sigma_w^2 \mathbf{I}_m$.

Then, the computing module of the spacecraft processes the sensing data and calculates the control command. Since the LQR-based control design is based on well-established control theory, the optimal control input, i.e., $\mathbf{u}_{k,i}$, can be calculated by solving a well-defined optimization problem.

Afterward, the mother spacecraft works as the BS to distribute control commands to the daughter probes. They are all equipped with a single antenna. According to [27], the near planet link has similar characteristics as the near Earth link. The detailed model depends on the planetary conditions, such as the presence of atmosphere and surface dust. To ensure the communication reliability, it is advisable to incorporate a certain electrical level allowance. We thereby adopt a large-scale model that considers both the line-of-sight and nonline-of-sight conditions of the near Earth link to model the near planet link [28]

$$PL[dB] = P_{Los}[FSPL + SF_1] + (1 - P_{Los})[FSPL + SF_2 + CL], \quad (3)$$

where P_{Los} is the line-of-sight probability, $FSPL$ is the free space path loss, SF_1 and SF_2 are the fading margins reserved for the shadowing fading, and CL is the clutter effect-introduced loss. The atmospheric effect is neglected by taking

Mars as an example, whose atmosphere is much thinner than that of Earth [27]. The computing formula of $FSPL$ is

$$FSPL(d_k, f_c) \triangleq 32.45 + 20 \log_{10}(f_c) + 20 \log_{10} d_k, \quad (4)$$

where d_k (m) is the distance between the spacecraft and the k th daughter probe and f_c (MHz) is the carrier frequency. In addition, we calculate the antenna gain of the spacecraft by the following expression [29]

$$G_k = G_{\max} \left(\frac{J_1(u_k)}{2u_k} + 36 \frac{J_3(u_k)}{u_k^3} \right)^2, \quad (5)$$

where $J_1(\cdot)$ and $J_3(\cdot)$ are the first-kind Bessel functions of order 1 and 3, G_{\max} is the maximum antenna gain, and u_k is given by

$$u_k = \frac{2.07123 \sin \theta_k}{\sin \theta_{3dB}}, \quad (6)$$

where θ_{3dB} is the one-sided half-power beam width and θ_k is the off-axis angle. Based on (3) and (5), the channel gain g_k is calculated as

$$g_k = G_k 10^{\frac{-PL[dB]}{10}}. \quad (7)$$

In addition, given the cycle time constraint, spacecraft-probe downlink works in the FBL regime such that the command can be timely delivered within the limited time window. The achievable rate expression in the FBL regime is given by [30]

$$r(n_k, p_k) \approx \log_2 \left(1 + \frac{g_k p_k}{\sigma^2} \right) - \sqrt{\frac{V(p_k)}{n_k}} Q^{-1}(\epsilon_k), \quad (8)$$

where n_k is the transmit block length, p_k is the transmit power, σ^2 is the noise variance, ϵ_k is the transmission error probability, $Q^{-1}(\cdot)$ is the inverse of the Q function, i.e., $Q(x) = \frac{1}{\sqrt{2\pi}} \int_x^\infty e^{-\frac{t^2}{2}} dt$, and $V(p_k)$ is the channel dispersion, which is approximated by the following expression [31]

$$V(p_k) \approx (\log_2 e)^2 \left(1 - \frac{1}{\left(1 + \frac{g_k p_k}{\sigma^2} \right)^2} \right). \quad (9)$$

Based on (8), the transmit bits per cycle, named as cycle rate, is calculated by

$$R(n_k, p_k) \approx (1 - \epsilon_k) \left(n_k \log_2 \left(1 + \frac{g_k p_k}{\sigma^2} \right) - \sqrt{n_k V(p_k)} Q^{-1}(\epsilon_k) \right). \quad (10)$$

Upon receiving control commands, the probe takes control actions, leading the system’s evolution as described by (1).

To ensure the above \mathbf{SC}^3 processes are finished within the cycle time, denoted as T_k^0 , it is necessary to satisfy

$$t_k^S + t_k^{Cm} + t_k^{Cp} + t_k^A \leq T_k^0, \quad n_k \in \mathbb{N}^+, \quad (11)$$

where t_k^S , t_k^{Cm} , t_k^{Cp} and t_k^A are the time for sensing, communication, computing and control. For simplicity, the time for sensing, computing and control is predetermined in this paper. Assuming the K \mathbf{SC}^3 loops are allocated with orthogonal subchannels with an equal bandwidth B , the communication-introduced latency is given by

$$t_k^{Cm} = \frac{n_k}{B} + \tau_k, \quad (12)$$

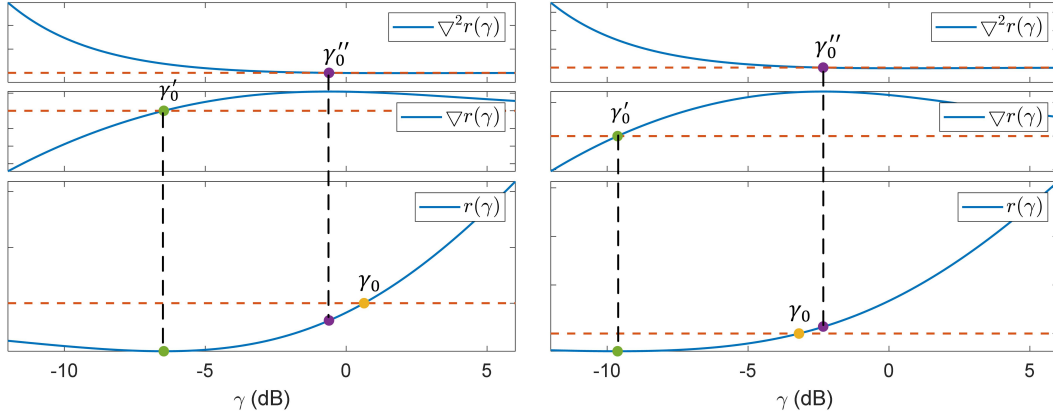


Fig. 3. Curves of the achievable rate in the FBL regime, its first derivative and second derivative. Related parameters are given by $\epsilon = 10^{-6}$, $n = 30$ for the left figure and $\epsilon = 10^{-6}$, $n = 80$ for the right figure.

where $\frac{n_k}{B}$ is the transmission delay and τ_k is the electromagnetic propagation delay, which is determined by the distance between the spacecraft and the probe, denoted as d_k ,

$$\tau_k = \frac{d_k}{c}, \quad (13)$$

where c is the speed of light. On this basis, (11) can be simplified into a constraint of the block length

$$\frac{n_k}{B} \leq T_k, \quad n_k \in \mathbb{N}^+, \quad (14)$$

where $T_k \triangleq T_k^0 - t_k^S - t_k^{CP} - t_k^A - \tau_k$.

Moving forward, we use the LQR cost to measure the closed-loop control performance, which is calculated by

$$l_k = \limsup_{N \rightarrow \infty} \mathbb{E} \left[\sum_{i=1}^N (\mathbf{x}_{k,i}^T \mathbf{Q}_k \mathbf{x}_{k,i} + \mathbf{u}_{k,i}^T \mathbf{R}_k \mathbf{u}_{k,i}) \right], \quad (15)$$

where \mathbf{Q}_k and \mathbf{R}_k are positive semidefinite matrices. They are used to balance the cost of the state derivation and control input. According to [15], the cycle rate needs to satisfy the following stable condition such that the controlled system can be stabilized

$$R(n_k, p_k) \geq \log_2 |\det \mathbf{A}_k|, \quad (16)$$

where $\log_2 |\det \mathbf{A}_k|$ is the intrinsic entropy, which quantifies the system instability level. On the premise that (16) is satisfied, the finite cycle rate constructs a lower bound of the LQR cost [17]

$$l_k \geq \frac{m |\det \mathbf{N}_k \mathbf{M}_k|^{\frac{1}{m}}}{2^{\frac{2}{m}(R(n_k, p_k) - \log_2 |\det \mathbf{A}_k|) - 1} + \text{tr}(\mathbf{\Sigma}_{\mathbf{v}_k} \mathbf{S}_k) + \text{tr}(\mathbf{\Sigma}_k \mathbf{A}_k^T \mathbf{M}_k \mathbf{A}_k)}, \quad (17)$$

where

$$\mathbf{S}_k = \mathbf{Q}_k + \mathbf{A}_k^T (\mathbf{S}_k - \mathbf{M}_k) \mathbf{A}_k, \quad (18a)$$

$$\mathbf{M}_k = \mathbf{S}_k^T \mathbf{B}_k (\mathbf{R}_k + \mathbf{B}_k \mathbf{S}_k \mathbf{B}_k)^{-1} \mathbf{B}_k^T \mathbf{S}_k, \quad (18b)$$

$$\mathbf{N}_k = \mathbf{A}_k \mathbf{\Sigma}_k \mathbf{A}_k^T - \mathbf{\Sigma}_k + \mathbf{\Sigma}_{\mathbf{v}_k}. \quad (18c)$$

$\mathbf{\Sigma}_k$ is calculated by the following expression

$$\mathbf{\Sigma}_k = \mathbf{P}_k - \mathbf{P}_k \mathbf{C}_k^T (\mathbf{C}_k \mathbf{P}_k \mathbf{C}_k^T + \mathbf{\Sigma}_{\mathbf{w}_k})^{-T} \mathbf{C}_k \mathbf{P}_k^T. \quad (19)$$

\mathbf{P}_k is the solution to the algebraic Riccati equation

$$\begin{aligned} \mathbf{P}_k = & \mathbf{A}_k \mathbf{P}_k \mathbf{A}_k^T + \mathbf{\Sigma}_{\mathbf{v}_k} \\ & - \mathbf{A}_k \mathbf{P}_k \mathbf{C}_k^T (\mathbf{C}_k \mathbf{P}_k \mathbf{C}_k^T + \mathbf{\Sigma}_{\mathbf{w}_k})^{-T} \mathbf{C}_k \mathbf{P}_k^T \mathbf{A}_k^T. \end{aligned} \quad (20)$$

According to [17], (17) is approximately reachable. We thus define our objective function, denoted as the rate-cost function, as follows

$$\begin{aligned} L(n_k, p_k) \triangleq & \frac{m |\det \mathbf{N}_k \mathbf{M}_k|^{\frac{1}{m}}}{2^{\frac{2}{m}(R(n_k, p_k) - \log_2 |\det \mathbf{A}_k|) - 1} - 1} \\ & + \text{tr}(\mathbf{\Sigma}_{\mathbf{v}_k} \mathbf{S}_k) + \text{tr}(\mathbf{\Sigma}_k \mathbf{A}_k \mathbf{M}_k \mathbf{A}_k^T). \end{aligned} \quad (21)$$

whose definition domain is restricted by the stable condition (16). As we can see, $L(n_k, p_k)$ establishes a fundamental relationship between the LQR cost and the communication cycle rate. This relationship enables us to optimize the spacecraft-probe downlink within SC^3 loops, which is detailed in the next Section.

III. THE SPACECRAFT-PROBE DOWNLINK OPTIMIZATION

Compared with the DSC between the spacecraft and the Earth center, the base station (BS) used for spacecraft-probe communication is relatively lightweight. The limited transmit power of the onboard BS and strict cycle time constraint lead to a limited cycle rate of the spacecraft-probe downlink. This further impacts the control task performance. To address this challenge, we propose a spacecraft-probe downlink optimization scheme. This scheme aims to minimize the LQR cost and takes the transmit power and block length as optimization variables

$$(P1) \quad \min_{n_k, p_k \geq 0} \sum_{k=1}^K L(n_k, p_k) \quad (22a)$$

$$\text{s.t.} \quad R(n_k, p_k) \geq \log_2 |\det \mathbf{A}_k|, \quad \forall k, \quad (22b)$$

$$\frac{n_k}{B} \leq T_k, \quad n_k \in \mathbb{N}^+, \quad (22c)$$

$$\sum_{k=1}^K p_k \leq P_{\max}. \quad (22d)$$

(P1) is a nonlinear mixed-integer problem. First, the optimal block length is determined by T_k

$$n_k^* = \lfloor BT_k \rfloor. \quad (23)$$

This is because $L(n_k, p_k)$ is a decreasing function of n_k . We can easily prove this by the rule of the monotonicity of composite functions, as the rate-cost function decreases with the cycle rate and the cycle rate decreases with the block length. After determining the block length, the remaining power allocation problem is given by

$$(P2) \quad \min_{p_k \geq 0} \sum_{k=1}^K L(p_k) \quad (24a)$$

$$\text{s.t.} \quad R(p_k) \geq \log_2 |\det \mathbf{A}_k|, \quad \forall k, \quad (24b)$$

$$\sum_{k=1}^K p_k \leq P_{\max}, \quad (24c)$$

where $R(p_k) \triangleq R(n_k^*, p_k)$ and $L(p_k) \triangleq L(n_k^*, p_k)$ are two complex expressions of the transmit power. To solve this problem, we first analyze their monotonicity and convexity-concavity. For the cycle rate $R(p_k)$, we analyze the property of the achievable rate expression $r(p_k) \triangleq r(n_k^*, p_k)$, as shown in (8). They have the same property with respect to the transmit power. For ease of expression, we rewrite $r(p_k)$ as a function of the signal-to-noise ratio (SNR), denoted as γ

$$r(\gamma) = \log_2(1 + \gamma) - \eta \sqrt{V(\gamma)}, \quad (25)$$

where $\eta \triangleq \sqrt{\frac{1}{n^*} Q^{-1}(\epsilon)}$ and the subscript k is omitted for simplicity. Since $r(\gamma)$ cannot be negative in practice, we thereby discuss its monotonicity and concavity-convexity in the region of $r(\gamma) \geq 0$, which is given by **Theorem 1**.

Theorem 1: Denote the zero-crossing point of $r(\gamma)$ as γ_0 .

- 1) $r(\gamma)$ is monotonically increasing with γ in $[\gamma_0, +\infty)$.
- 2) The convexity-concavity of $r(\gamma)$ is given by

$$\begin{cases} r(\gamma) \text{ is convex-concave in } [\gamma_0, +\infty), & \eta < \hat{\eta}, \\ r(\gamma) \text{ is concave in } [\gamma_0, +\infty), & \eta \geq \hat{\eta}. \end{cases} \quad (26)$$

where $\hat{\eta} \triangleq \frac{(1+\hat{\gamma}) \ln(1+\hat{\gamma})}{\sqrt{\hat{\gamma}^2 + 2\hat{\gamma}}}$ and $\hat{\gamma}$ is the zero-crossing point of the following equation

$$\ln(1 + \gamma) - \frac{(1 + \gamma)(\gamma^2 + 2\gamma)^2}{3\gamma^2 + 6\gamma + 1} = 0. \quad (27)$$

Proof: See Appendix A. ■

In Fig. 3, we illustrate two examples of $r(\gamma)$ along with its first-order derivative $\nabla r(\gamma)$ and second-order derivative $\nabla^2 r(\gamma)$. The zero-crossing points of $\nabla r(\gamma)$ and $\nabla^2 r(\gamma)$ are denoted as γ'_0 and γ''_0 , respectively. It is important to note that γ'_0 is the monotonicity turning point of $r(\gamma)$ and γ''_0 is the inflection point of $r(\gamma)$. The values of γ'_0 and γ''_0 compared with γ_0 determine the monotonicity and the concavity-convexity of $r(\gamma)$ in $[\gamma_0, +\infty)$. Observing both figures, we can see that $\gamma_0 > \gamma'_0$ in both cases. This shows that the two presented examples are monotonically increasing in $[\gamma_0, +\infty)$. Moreover, the left example demonstrates the concave nature of

Algorithm 1 The Proposed Spacecraft-Probe Downlink Optimization Algorithm

Input: The number of SC³ loops: K ;

Sensing related parameter: $\Sigma_{\mathbf{w}_k}$;

Communication related parameters: $B, P_{\max}, \epsilon_k, d_k, \sigma^2, \alpha, \beta_0$;

Control related parameters: $\mathbf{A}_k, \mathbf{B}_k, \mathbf{Q}_k, \mathbf{R}_k, \Sigma_{\mathbf{v}_k}, m$;

Cycle time: T_k^0 and the time for sensing, computing, and control: $T_k^S, T_k^C, \text{ and } T_k^A$.

Iteration termination threshold: ϵ .

1: Calculate the transmission time according to (14);

2: Calculate $\mathbf{S}_k, \mathbf{M}_k, \mathbf{N}_k$, and Σ_k according to (18)-(20);

3: Calculate the optimal block length n_k^* according to (23);

4: Calculate the stable condition threshold p_k^{th} according to (29);

5: Obtain the optimal transmit power p_k^* by solving (P3);

Output: the optimal block length n_k^* and transmit power p_k^* .

$r(\gamma)$ in $[\gamma_0, +\infty)$, as γ_0 exceeds γ''_0 . Conversely, in the right example, γ_0 is smaller than γ''_0 , illustrating the convex-concave property of $r(\gamma)$.

Moving forward, based on the monotonicity of $r(\gamma)$ in $[\gamma_0, +\infty)$, constraint (24b) can be simplified into a threshold form

$$p_k \geq p_k^{th}, \quad \forall k, \quad (28)$$

where p_k^{th} is the solution to the following equation

$$R(p_k) - \log_2 |\det \mathbf{A}_k| = 0, \quad (29)$$

which can be found by the dichotomy method. Thus, (P2) is simplified as

$$(P3) \quad \min_{p_k \geq 0} \sum_{k=1}^K L(p_k) \quad (30a)$$

$$\text{s.t.} \quad p_k \geq p_k^{th}, \quad \forall k, \quad (30b)$$

$$\sum_{k=1}^K p_k \leq P_{\max}. \quad (30c)$$

In (P3), the rate-cost function is a composite function that contains exponential, fractional, and logarithmic terms. Moving forward, we have **Theorem 2**.

Theorem 2: The rate-cost function is a concave function with respect to the transmit power.

Proof: See Appendix B. ■

Based on **Theorem 2**, we can conclude that (P3) is convex, which can be easily solved by the convex optimization tool. The corresponding algorithm is summarized in **Algorithm 1**.

IV. COMPARISONS WITH TRADITIONAL COMMUNICATION SCHEMES

In this section, we will compare the proposed scheme with two communication-oriented schemes: the max-sum rate scheme and the max-min rate scheme. The optimal block length is calculated as before so we will only focus on the power allocation. We will first derive the closed-form solutions of all three schemes. Subsequently, we will analyze their power allocation principles.

A. Communication-Oriented Power Allocation

From the perspective of communication, the sum rate and the min rate are two important metrics that reflect the system efficiency and fairness, respectively. The corresponding schemes are given by

$$(PA) \max_{p_k \geq 0} \sum_{k=1}^K R(p_k) \quad (31a)$$

$$\text{s.t. } R(p_k) \geq \log_2 |\det \mathbf{A}_k|, \forall k, \quad (31b)$$

$$\sum_{k=1}^K p_k \leq P_{\max}, \quad (31c)$$

$$(PB) \max_{p_k \geq 0} \min_k R(p_k) \quad (32a)$$

$$\text{s.t. } R(p_k) \geq \log_2 |\det \mathbf{A}_k|, \forall k, \quad (32b)$$

$$\sum_{k=1}^K p_k \leq P_{\max}. \quad (32c)$$

As stated in **Theorem 1**, the cycle rate $R(p_k)$ is not necessarily concave to the transmit power. This indicates (PA) and (PB) are both non-convex. To address this obstacle, we employ the first-order Taylor expansion to linearize the nonconvex term in the cycle rate, i.e., $\sqrt{V(p_k)}$. Considering a fixed point \hat{p}_k , the Taylor expansion expression is given by

$$R(p_k | \hat{p}_k) = (1 - \epsilon_k) \left[n_k^* \log_2 \left(1 + \frac{g_k p_k}{\sigma^2} \right) - \sqrt{n_k^*} Q^{-1}(\epsilon_k) \times \left(\sqrt{V(\hat{p}_k)} + \nabla \sqrt{V(\hat{p}_k)} (p_k - \hat{p}_k) \right) \right], \quad (33)$$

where

$$\nabla \sqrt{V(\hat{p}_k)} = \frac{\log_2(e) \frac{g_k}{\sigma^2}}{\left(1 + \frac{g_k \hat{p}_k}{\sigma^2} \right)^2 \sqrt{\left(\frac{g_k \hat{p}_k}{\sigma^2} \right)^2 + 2 \frac{g_k \hat{p}_k}{\sigma^2}}}. \quad (34)$$

Thus, we solve (PA) and (PB) in an iterative way. The problems at the i th iteration are formulated as

$$(PA-2) \max_{p_k \geq 0} \sum_{k=1}^K R(p_k | p_k^{i-1}) \quad (35a)$$

$$\text{s.t. } p_k \geq p_k^{th}, \forall k, \quad (35b)$$

$$\sum_{k=1}^K p_k \leq P_{\max}. \quad (35c)$$

$$(PB-2) \max_{p_k \geq 0} \min_k R(p_k | p_k^{i-1}), \quad (36a)$$

$$\text{s.t. } p_k \geq p_k^{th}, \forall k, \quad (36b)$$

$$\sum_{k=1}^K p_k \leq P_{\max}. \quad (36c)$$

where (35b) and (36b) are derived from the stable condition (29) and p_k^{i-1} is the solution obtained in the $(i-1)$ th iteration. The algorithm converges as a result of the monotonicity and boundedness of generated solutions. We summarize the corresponding algorithm in **Algorithm 2**.

Algorithm 2 The Max-Sum Rate and Max-Min Rate Power Allocation Algorithm

Input: The number of SC^3 loops: K ;
Sensing related parameter: $\Sigma_{\mathbf{w}_k}$;
Communication related parameters: $B, P_{\max}, \epsilon_k, d_k, \sigma^2, \alpha, \beta_0$;
Control related parameters: $\mathbf{A}_k, \mathbf{B}_k, \mathbf{Q}_k, \mathbf{R}_k, \Sigma_{\mathbf{v}_k}, m$;
Cycle time: T_k^0 ; the time for sensing, computing, and control: $T_k^S, T_k^C, \text{ and } T_k^A$;
Iteration termination threshold: ϵ .

- 1: Calculate $\mathbf{S}_k, \mathbf{M}_k, \mathbf{N}_k$, and Σ_k according to (18)-(20);
- 2: Calculate the transmission time according to (14);
- 3: Calculate the optimal block length n_k^* according to (23);
- 4: Calculate the stable condition threshold p_k^{th} according to (29);
- 5: *Initialization:* $i = 0$ and $p_k^i = p_k^{th}$;
- 6: **repeat**
- 7: $i = i + 1$;
- 8: Obtain $p_k^{(i)}$ by solving (PA-2) and (PB-2);
- 9: **until** $\frac{\left| \sum_{k=1}^K R(p_k^{(i)}) - \sum_{k=1}^K R(p_k^{(i-1)}) \right|}{\sum_{k=1}^K R(p_k^{(i-1)})} \leq \epsilon$ for (PA);
and $\frac{\left| \min_k R(p_k^{(i)}) - \min_k R(p_k^{(i-1)}) \right|}{\min_k R(p_k^{(i-1)})} \leq \epsilon$ for (PB).

Output: the optimal transmit power p_k^* .

B. Approximate Closed-Form Solutions

In this subsection, we derive the approximate closed-form solutions of these three schemes. We assume all SC^3 loops have the same transmission time, i.e., $T_k = T$. According to (23), the optimal length is $n = \lfloor BT \rfloor$. In addition, on the condition that the received SNR is greater than 5 dB, i.e., $10 \log_{10} \left(\frac{g_k p_k}{\sigma^2} \right) \geq 5$ dB, we can approximate the cycle rate $R(p_k)$ as [32]

$$R(p_k) = n \log_2 \left(1 + \frac{g_k p_k}{\sigma^2} \right) - \sqrt{n} \log_2(e) Q^{-1}(\epsilon_k), \quad (37)$$

Furthermore, when the system is in the assure-to-be-stable region, i.e., $R(p_k) \gg \log_2 |\det \mathbf{A}_k|$, the approximation to the rate-cost function is

$$\begin{aligned} L(p_k) &= \frac{m |\det \mathbf{N}_k \mathbf{M}_k|^{\frac{1}{m}}}{2^{\frac{2}{m}} (R(p_k) - \log_2 |\det \mathbf{A}_k|) - 1} \\ &\quad + \text{tr}(\Sigma_{\mathbf{v}_k} \mathbf{S}_k) + \text{tr}(\Sigma_k \mathbf{A}_k \mathbf{M}_k \mathbf{A}_k) \\ &\approx \frac{m |\det \mathbf{N}_k \mathbf{M}_k|^{\frac{1}{m}}}{2^{\frac{2}{m}} (R(p_k) - \log_2 |\det \mathbf{A}_k|)} \\ &\quad + \text{tr}(\Sigma_{\mathbf{v}_k} \mathbf{S}_k) + \text{tr}(\Sigma_k \mathbf{A}_k \mathbf{M}_k \mathbf{A}_k) \\ &\approx \frac{m |\det \mathbf{N}_k \mathbf{M}_k|^{\frac{1}{m}} |\det \mathbf{A}_k|^{\frac{2}{m}} e^{\frac{2\sqrt{n}}{m}} Q^{-1}(\epsilon_k)}{(1 + \frac{g p_k}{\sigma^2})^{\frac{2n}{m}}} \\ &\quad + \text{tr}(\Sigma_{\mathbf{v}_k} \mathbf{S}_k) + \text{tr}(\Sigma_k \mathbf{A}_k \mathbf{M}_k \mathbf{A}_k). \end{aligned} \quad (38)$$

By testing the Slater condition, it is easy to find that the strong duality holds for (P3). Solving its dual problem yields the same optimal solution. The dual problem is given by

$$(P4) \max_{\lambda} \min_{p_k \geq 0} \sum_{k=1}^K L(p_k) + \lambda \left(\sum_{k=1}^K p_k - P_{\max} \right) \quad (39a)$$

$$\text{s.t. } \lambda \geq 0, \quad (39b)$$

where λ is the Lagrangian multiplier. The stable condition is omitted for it is satisfied in advance in the assure-to-be-stable

region. The Karush-Kuhn-Tucker (KKT) conditions of (P4) are given by

$$\begin{cases} \frac{\partial L(p_k)}{\partial p_k} + \lambda|_{p_k=p_k^*} = 0, \forall k, & (40a) \\ \sum_{k=1}^K p_k - P_{\max} = 0, & (40b) \\ \lambda \geq 0, & (40c) \end{cases}$$

where the equality of (40b) comes from the monotonicity of $L(p_k)$. Based on the approximation of $L(p_k)$ given in (38), we calculate $\frac{\partial L(p_k)}{\partial p_k}$ and obtain that

$$p_k^*(\lambda) = \left(\frac{\sigma^2}{g_k}\right)^{\frac{2n}{2n+m}} \left(\frac{2nG_k}{\lambda}\right)^{\frac{m}{2n+m}} e^{\frac{2\sqrt{n}Q^{-1}(\epsilon_k)}{2n+m}} - \frac{\sigma^2}{g_k}, \quad (41)$$

where $G_k \triangleq |\det \mathbf{N}_k \mathbf{M}_k|^{\frac{1}{m}} |\det \mathbf{A}_k|^{\frac{2}{m}}$, which represents the sensing-and-control related parameter. By substituting (41) into (40b), we can further obtain that

$$\left(\frac{1}{\lambda}\right)^{\frac{m}{2n+m}} = \frac{P_{\max} + \sum_{i=1}^K \frac{\sigma^2}{g_i}}{\sum_{i=1}^K \left(\frac{\sigma^2}{g_i}\right)^{\frac{2n}{2n+m}} (2nG_i)^{\frac{m}{2n+m}} e^{\frac{2\sqrt{n}Q^{-1}(\epsilon_i)}{2n+m}}}. \quad (42)$$

Combining (42) and (41), the closed-form solution to the proposed scheme is

$$p_k^* = \left(P_{\max} + \sum_{i=1}^K \frac{\sigma^2}{g_i}\right) \frac{\left(\frac{\sigma^2}{g_k}\right)^{\frac{2n}{2n+m}} e^{\frac{2\sqrt{n}Q^{-1}(\epsilon_k)}{2n+m}} G_k^{\frac{m}{2n+m}}}{\sum_{i=1}^K \left(\frac{\sigma^2}{g_i}\right)^{\frac{2n}{2n+m}} e^{\frac{2\sqrt{n}Q^{-1}(\epsilon_i)}{2n+m}} G_i^{\frac{m}{2n+m}}} - \frac{\sigma^2}{g_k}. \quad (43)$$

Furthermore, we extend this closed-form solution to a more general case by substituting n with n_k^* . Thus, (43) can be applied to the case that different loops have different cycle time. The corresponding solution is quite accurate when the cycle time difference of different \mathbf{SC}^3 loops is not significant.

Moving forward, we derive the closed-form solutions to two communication-oriented schemes. Using the high-SNR approximation in (37), (PA) and (PB) become two convex problems. As for (PA), if there is no stable condition (31b), the optimal solution can be obtained using the classical water-filling method [33, Ch 9.4]

$$p_k^* = \left[\frac{1}{\lambda} - \frac{\sigma^2}{g_k}\right]^+, \quad (44)$$

where $[x]^+ = \max\{x, 0\}$, λ is chosen to satisfy $\sum_{k=1}^K p_k = P_{\max}$. On this basis, it is easy to derive the closed-form solution to (PA)

$$p_k^* = \max\left(\left[\frac{1}{\lambda} - \frac{\sigma^2}{g_k}\right]^+, p_k^{th}\right), \quad (45)$$

where λ is chosen to satisfy $\sum_{k=1}^K p_k = P_{\max}$.

As for the max-min rate scheme, if there is no stable condition (32b), the optimal solution to (PB) satisfies

$$R(p_1^*) = R(p_2^*) = \dots = R(p_K^*) = \lambda, \quad (46)$$

where λ is an auxiliary variable. This is because if (46) does not hold, the minimal cycle rate of the K \mathbf{SC}^3 loops could

be further improved by reducing the allocated transmit power of other loops. Based on (46), we can obtain that

$$p_k^* = 2^{\frac{\lambda}{n}} \left(\frac{\sigma^2}{g_k}\right) e^{\frac{Q^{-1}(\epsilon_k)}{\sqrt{n}}} - \frac{\sigma^2}{g_k}. \quad (47)$$

By substituting (47) into $\sum_{k=1}^K p_k^* = P_{\max}$, we can obtain that

$$2^{\frac{\lambda}{n}} = \frac{P_{\max} + \sum_{i=1}^K \frac{\sigma^2}{g_i}}{\sum_{i=1}^K \frac{\sigma^2}{g_i} e^{\frac{Q^{-1}(\epsilon_i)}{\sqrt{n}}}}. \quad (48)$$

We further substitute (48) into (47). Then, the closed-form solution of the transmit power is given by

$$p_k^* = \left(P_{\max} + \sum_{i=1}^K \frac{\sigma^2}{g_i}\right) \frac{\frac{\sigma^2}{g_k} e^{\frac{Q^{-1}(\epsilon_k)}{\sqrt{n}}}}{\sum_{i=1}^K \frac{\sigma^2}{g_i} e^{\frac{Q^{-1}(\epsilon_i)}{\sqrt{n}}}} - \frac{\sigma^2}{g_k}. \quad (49)$$

On this basis, it is easy to obtain the closed-form solution to (PB) by taking the stable condition into account

$$p_k^* = \max\left[\left(\lambda + \sum_{i=1}^K \frac{\sigma^2}{g_i}\right) \frac{\frac{\sigma^2}{g_k} e^{\frac{Q^{-1}(\epsilon_k)}{\sqrt{n}}}}{\sum_{i=1}^K \frac{\sigma^2}{g_i} e^{\frac{Q^{-1}(\epsilon_i)}{\sqrt{n}}}} - \frac{\sigma^2}{g_k}, p_k^{th}\right] \quad (50)$$

where λ is chosen to satisfy $\sum_{k=1}^K p_k^* = P_{\max}$. In addition, if P_{\max} is large enough such that $p_k \geq p_k^{th}$ is satisfied, the optimal solution is exactly (49).

C. Analysis of Power Allocation Principles

Comparing the closed-form solutions to the proposed scheme, the max-sum rate scheme and the max-min rate scheme, we have the following observations.

- 1) The proposed scheme provides a way to account for sensing, computing, and control factors in communication design. According to (43), the \mathbf{SC}^3 loops with less accurate sensing and higher instability (corresponding to a larger G_k) are assigned more transmit power. In contrast, communication-oriented schemes overlook these crucial factors as they solely focus on communication performance.
- 2) In terms of channel conditions, the proposed scheme and the max-min rate scheme exhibit a similar power allocation pattern. They allocate more power to the \mathbf{SC}^3 loops with poorer channel conditions. Conversely, the max-sum rate scheme allocates more power to those \mathbf{SC}^3 loops with better channels.

In addition to the similar allocation principle between the proposed scheme and the max-min rate scheme of channel conditions, we further find their equivalence for time-insensitive tasks, which is concluded by the following **Theorem**.

Theorem 3: When $n \gg m$, the following modified max-min rate scheme yields the same power allocation solution as the proposed scheme

$$(PC) \max_{p_k \geq 0} \min_k R(p_k) - \frac{m}{2} \log_2(G_k) \quad (51a)$$

$$s.t. R(p_k) \geq \log_2 |\det \mathbf{A}_k|, \forall k, \quad (51b)$$

$$\sum_{k=1}^K p_k \leq P_{\max}. \quad (51c)$$

In addition, when the block length n goes to infinity, the max-min rate scheme yields the same solution as the proposed scheme.

Proof: When $n \gg m$, we have that $\lim_{n \gg m} 2n + m = 2n$.

Then, the closed-form solution of the proposed scheme (43) has the following approximation

$$\begin{aligned} & \lim_{n \gg m} \left[(P_{\max} + \sum_{i=1}^K \frac{\sigma^2}{g_i}) \frac{(\frac{\sigma^2}{g_k})^{\frac{2n}{2n+m}} e^{\frac{2\sqrt{n}Q^{-1}(\epsilon_k)}{2n+m}} G_k^{\frac{m}{2n+m}}}{\sum_{i=1}^K (\frac{\sigma^2}{g_i})^{\frac{2n}{2n+m}} e^{\frac{2\sqrt{n}Q^{-1}(\epsilon_i)}{2n+m}} G_i^{\frac{m}{2n+m}}} - \frac{\sigma^2}{g_k} \right], \\ & = (P_{\max} + \sum_{i=1}^K \frac{\sigma^2}{g_i}) \frac{\frac{\sigma^2}{g_k} e^{\frac{Q^{-1}(\epsilon_k)}{\sqrt{n}}} G_k^{\frac{m}{2n}}}{\sum_{i=1}^K \frac{\sigma^2}{g_i} e^{\frac{Q^{-1}(\epsilon_i)}{\sqrt{n}}} G_i^{\frac{m}{2n}}} - \frac{\sigma^2}{g_k}. \end{aligned} \quad (52)$$

By comparing (52) with the closed-form solution of the max-min rate scheme (49), it is easy to find that (52) is the closed-form solution to (PC). In addition, when the block length n goes to infinity, the following approximations can be made

$$\begin{aligned} \lim_{n \rightarrow +\infty} \frac{2n}{2n+m} &= 1, \\ \lim_{n \rightarrow +\infty} \frac{2\sqrt{n}}{2n+m} &= \frac{1}{\sqrt{n}}. \end{aligned} \quad (53)$$

Then, the closed-form solution of the proposed scheme (43) can be further simplified into

$$\begin{aligned} & \lim_{n \gg m} \left[(P_{\max} + \sum_{i=1}^K \frac{\sigma^2}{g_i}) \frac{(\frac{\sigma^2}{g_k})^{\frac{2n}{2n+m}} e^{\frac{2\sqrt{n}Q^{-1}(\epsilon_k)}{2n+m}} G_k^{\frac{m}{2n+m}}}{\sum_{i=1}^K (\frac{\sigma^2}{g_i})^{\frac{2n}{2n+m}} e^{\frac{2\sqrt{n}Q^{-1}(\epsilon_i)}{2n+m}} G_i^{\frac{m}{2n+m}}} - \frac{\sigma^2}{g_k} \right], \\ & = (P_{\max} + \sum_{i=1}^K \frac{\sigma^2}{g_i}) \frac{\frac{\sigma^2}{g_k} e^{\frac{Q^{-1}(\epsilon_k)}{\sqrt{n}}}}{\sum_{i=1}^K \frac{\sigma^2}{g_i} e^{\frac{Q^{-1}(\epsilon_i)}{\sqrt{n}}}} - \frac{\sigma^2}{g_k}, \end{aligned} \quad (54)$$

which is the same as the solution to the max-min rate scheme (49). ■

Theorem 3 reveals the fairness-minded nature of the proposed scheme. To chase the minimal sum LQR cost, it guarantees a minimum level of performance for all loops, avoiding the ‘‘short-board effect’’ that drags down the overall system efficiency. In addition, the equivalence of the proposed scheme and the max-min rate scheme indicates that as the cycle time increases, the interdependence between communication and control gets weaker. Under this condition, the fairness-mined communication scheme yields the near-optimal solution. We can conclude that the proposed scheme is necessary for time-sensitive control tasks, while the max-min rate scheme is a good alternative for time-insensitive cases.

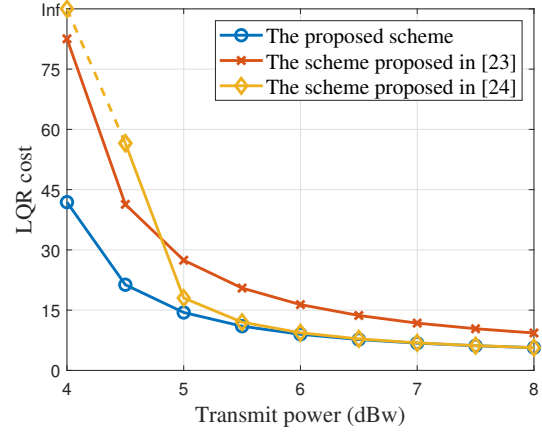


Fig. 4. Comparisons of the control performance under three optimization schemes in the low-power region.

V. SIMULATION RESULTS AND DISCUSSION

In the simulation, we assume there are $K = 4$ SC^3 loops. For sensing related parameters, we set $\mathbf{C}_k = \mathbf{I}_m$ and $\Sigma_{\mathbf{w}_k} = \mathbf{0}_m$. For control-related parameters, we set $m = 100$, $\mathbf{Q}_k = \mathbf{I}_m$, $\mathbf{R}_k = \mathbf{0}_m$, and $\Sigma_{\mathbf{v}_k} = 0.01 * \mathbf{I}_m$ [24]. The intrinsic entropy is given by $\log_2 |\det \mathbf{A}_k| = [48, 36, 24, 12]$. The control cycle time is $T_k^0 = 50$ ms and the time used for sensing, computing and control is 40 ms. Each SC^3 loop is allocated with a narrow frequency band of $B = 15$ kHz. The carrier frequency is $f_c = 2$ GHz, the noise variance is $\sigma^2 = -110$ dBm, and the transmission error probability is $\epsilon_k = 10^{-6}$. The maximal antenna gain is $G_{\max} = 23$ dBi and $\theta_{3\text{dB}} = 30^\circ$. We choose the rural scenario to model the planet environment and the channel related parameters are given by $P_{\text{Los}} = 91.9\%$, $SF_1 = 1.14$ dB, $SF_2 = 8.78$ dB and $CL = 18.42$ dB [28]. According to the height of the Mars orbit, we set the height of the spacecraft to 3000 km and the four probes are located [1000, 2000, 3000, 4000] km away from the horizontal projection point of the spacecraft. In the present figures, the dotted line represents the infinite LQR cost and the system is unstable in this situation.

In Fig. 4, we compare the proposed scheme with the schemes proposed in [23] and [24]. The scheme in [23] defined a new objective named the energy-to-control efficiency. We

thereby take $\frac{P_{\max} - \sum_{k=1}^K p_k}{\sum_{k=1}^K L(n_k, p_k)}$ as its objective for optimization. The

scheme in [24] took the LQR cost as the objective but used the Shannon capacity to calculate the cycle rate. It can be seen the scheme proposed in [24] performs the worst when $P_{\max} \leq 4.5$ dBw. This is attributed to its unawareness of the rate drop in the FBL regime. Some loops that should have been allocated with more power are under allocated. This results in system instability when the available power is greatly limited. As the power increases, the LQR cost under the scheme in [23] becomes the highest. This is due to its emphasis on energy efficiency. The control performance has to make a compromise to save power.

In Fig. 5, we compare the proposed scheme with three

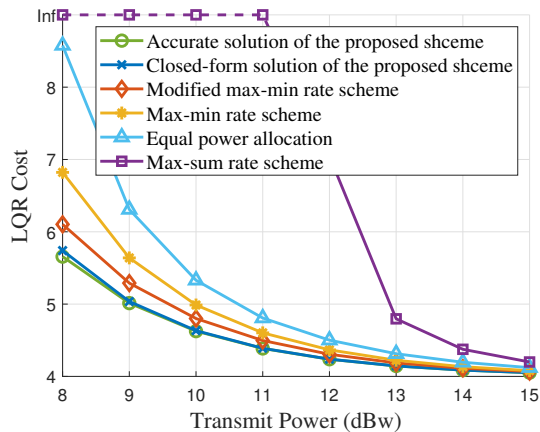


Fig. 5. Comparisons of the proposed scheme, the modified max-min rate scheme, the max-min rate scheme, the max-sum rate scheme and equal power allocation.

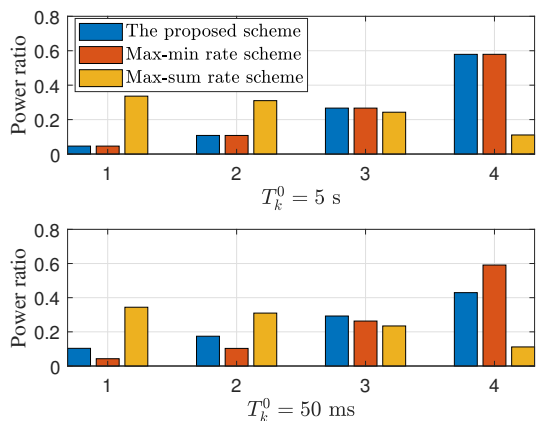


Fig. 6. The power allocation results under different schemes

communication-oriented schemes: the max-sum rate scheme, the max-min rate scheme, and the classical equal power allocation. The curves under the approximate closed-form solution of the proposed scheme (43) and the modified max-min rate scheme (PC) are also shown. It can be seen that the control performance of the approximate closed-form solution (43) is nearly the same as that of the accurate solution. The performance under the modified max-min rate scheme shows a small gap from the optimal one. In addition, we can also see that the max-min rate scheme outperforms the equal power allocation. Both of them further outperform the max-sum rate scheme. This is attributed to their different power allocation principles in terms of the channel condition. The max-min rate scheme holds a similar allocation principle as the proposed scheme, while the max-sum rate scheme follows an opposite allocation principle.

Furthermore, we present the power allocation results of the proposed scheme, the max-sum rate scheme, and the max-min rate scheme in Fig. 6. The maximal transmit power is set as $P_{\max} = 10$ dBw. It is evident that in both subfigures, the power ratio increases from loop one to four under the proposed scheme and the max-min rate scheme, while it

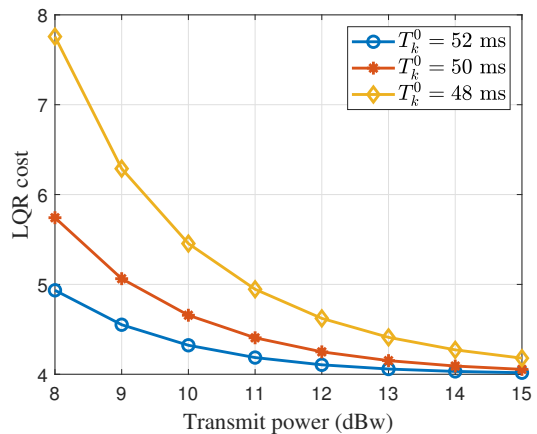


Fig. 7. Comparisons of the LQR cost under different cycle time

decreases under the max-sum rate scheme. This verifies our conclusions on their power allocation principles on channel conditions. In addition, when the cycle time is 50 ms, the proposed scheme allocates more power to SC^3 loops 1 ~ 3 compared to the max-min rate scheme. This is because we set $\log_2 |\det \mathbf{A}_k| = [48, 36, 24, 12]$. This adjustment is made to compensate for the intrinsic entropy difference. In the top subfigure, which shows the case of $T_k^0 = 5$ s, the power allocation results of the proposed scheme and the max-min rate scheme are nearly the same. In this situation, the intrinsic entropy difference has little impact on the communication design. This verifies our conclusions drawn in **Theorem 3**.

Next, we discuss the impacts of the cycle time on the control performance. The results are presented in Fig. 7. It can be seen that the cycle time primarily impacts the control performance in the lower power region. As the power increases, different curves converge to the same minimal value. This phenomenon stems from the fact that in the low power region, the limited cycle rate hinders the accuracy of transmit commands. Different cycle time leads to different cycle rates and, consequently, different control performances. While in the high-power region, all loops have an adequate cycle rate to deliver commands accurately. The control performances under different cycle time all go to the same optimum, making the cycle time less influential in this region.

In Fig. 8, we present the impacts of the sensing noise on the control performance. Different from the impact of cycle time, the LQR cost under different sensing noise would not converge to the same minimal value as the power increases. This reason is that the inaccurate sensing leads to the control command deviating from the accurate command. This inaccuracy can not be eliminated regardless of how excellent the communication is. In fact, in the flat region of these curves, the bottleneck of the SC^3 loop is no longer communication but sensing.

VI. CONCLUSIONS

In this paper, we have investigated the potential of the “mother-daughter structure” in unmanned space exploration. To improve the control performance of this “mother-daughter structure”, we have proposed a spacecraft-probe downlink

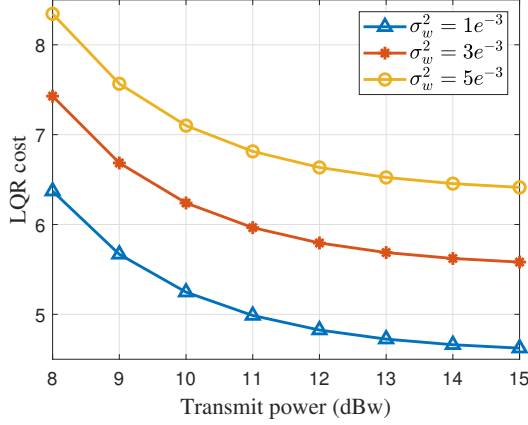


Fig. 8. Comparisons of the LQR cost under different sensing noise

optimization scheme, which takes the sum LQR cost of SC^3 loops as the objective. To tackle the formed nonlinear mixed-integer problem, we have analyzed the monotonicity and convexity of the achievable rate expression in the FBL regime and the rate-cost function. Based on their optimization-friendly properties, we have derived the optimal block length and transformed the power allocation problem into a convex problem. Moreover, we have derived the approximate closed-form solutions of the transmit power for the proposed scheme, the max-sum rate scheme, and the max-min rate scheme. Based on these closed-form solutions, we have revealed the equivalence between the proposed scheme and the max-min rate scheme for time-insensitive control tasks. We hope this work can attract more attention to the working regime of the SC^3 loop, which could activate the “mother-daughter structure” for future large-scale unmanned space exploration.

APPENDIX A PROOF OF Theorem 1

To prove the monotonicity and concavity-convexity of the achievable rate expression in the FBL regime, i.e., $r(\gamma)$, as shown in (25), we first calculate its first-order and second-order derivatives

$$\nabla r(\gamma) = \frac{\log_2 e}{\gamma + 1} \left(1 - \frac{\eta}{(\gamma + 1)\sqrt{\gamma^2 + 2\gamma}} \right), \quad (55)$$

$$\nabla^2 r(\gamma) = \frac{\log_2 e}{(\gamma + 1)^2} \left(\frac{2\eta}{(\gamma + 1)(\gamma^2 + 2\gamma)^{\frac{1}{2}}} + \frac{\eta(\gamma + 1)}{(\gamma^2 + 2\gamma)^{\frac{3}{2}}} - 1 \right). \quad (56)$$

On this basis, it can be proven that $\nabla r(\gamma)$ is thus first negative and then positive in $[0, +\infty)$, and we denote the zero-crossing point as γ'_0 . $r(\gamma)$ is monotonically decreasing in $[0, \gamma'_0)$ and monotonically increasing in $[\gamma'_0, +\infty)$. Since $r(\gamma)|_{\gamma=0} = 0$, $r(\gamma)$ is negative in $[0, \gamma'_0)$. Therefore, the zero-crossing point of $r(\gamma)$, i.e., γ_0 , is greater than γ'_0 . $r(\gamma)$ is monotonically increasing in $[\gamma_0, +\infty)$.

Similarly, it can be proven that $\nabla^2 r(\gamma)$ is first positive and then negative when $\gamma \in [0, +\infty)$. Denote its zero-crossing point as γ''_0 . $r(\gamma)$ is convex in $[0, \gamma''_0)$ and concave in $[\gamma''_0, +\infty)$. Therefore, whether $r(\gamma)$ is convex in $[\gamma_0, +\infty)$ is

determined by the relationship between γ_0 and γ''_0 . Since γ_0 is the zero point of $r(\gamma)$, we have

$$\begin{aligned} \log_2(\gamma_0 + 1) - \log_2(e)\eta\sqrt{1 - \frac{1}{(\gamma_0 + 1)^2}} &= 0 \\ \Rightarrow \eta &= \frac{(\gamma_0 + 1)\ln(\gamma_0 + 1)}{\sqrt{\gamma_0^2 + 2\gamma_0}}. \end{aligned} \quad (57)$$

On this basis, an auxiliary function is introduced as follows

$$f_1(\gamma) = \frac{(\gamma + 1)\ln(\gamma + 1)}{\sqrt{\gamma^2 + 2\gamma}}. \quad (58)$$

Similarly, since γ''_0 is the zero point of $\nabla^2 r(\gamma)$, we have that

$$\begin{aligned} \frac{2\eta}{(\gamma''_0 + 1)([\gamma''_0]^2 + 2\gamma''_0)^{\frac{1}{2}}} + \frac{\eta(\gamma''_0 + 1)}{([\gamma''_0]^2 + 2\gamma''_0)^{\frac{3}{2}}} - 1 &= 0 \\ \Rightarrow \eta &= \frac{(\gamma''_0 + 1)(\gamma''_0{}^2 + 2\gamma''_0)^{\frac{3}{2}}}{3\gamma''_0{}^2 + 6\gamma''_0 + 1}. \end{aligned} \quad (59)$$

Another auxiliary function is introduced as follows

$$f_2(\gamma) = \frac{(\gamma + 1)(\gamma^2 + 2\gamma)^{\frac{3}{2}}}{3\gamma^2 + 6\gamma + 1}. \quad (60)$$

The fact that there is only one zero point of $r(\gamma)$ (except 0) and $\nabla^2 r(\gamma)$ means that, for any $\eta > 0$, γ_0 and γ''_0 are the only solutions to $f_1(\gamma) = \eta$ and $f_2(\gamma) = \eta$. In other words, $f_1(\gamma)$ and $f_2(\gamma)$ are injective functions when $\gamma > 0$. Therefore, we can turn the comparison of γ_0 and γ''_0 into the comparison of $f_1(\gamma)$ and $f_2(\gamma)$. If η is in the region of $f_1(\gamma) > f_2(\gamma)$, $\gamma_0 < \gamma''_0$ holds, otherwise, $\gamma_0 \geq \gamma''_0$ holds. Then, we denote $f(\gamma) = f_1(\gamma) - f_2(\gamma)$

$$f(\gamma) = \frac{(\gamma + 1)}{\sqrt{\gamma^2 + 2\gamma}} \left[\ln(\gamma + 1) - \frac{(\gamma + 1)(\gamma^2 + 2\gamma)^2}{3\gamma^2 + 6\gamma + 1} \right].$$

It can be further proven that $f(\gamma)$ is first positive and then negative in $[0, +\infty)$. Denoting its zero-crossing point as $\hat{\gamma}$, we could draw the conclusion that

$$\begin{cases} f_1(\gamma) \geq f_2(\gamma), & \gamma \leq \hat{\gamma}, \\ f_1(\gamma) < f_2(\gamma), & \gamma > \hat{\gamma}. \end{cases} \quad (61)$$

Then, given the value of η , the relationship of γ_0 and γ''_0 can be judged by determining whether η is greater than $f_1(\hat{\gamma})$ (or $f_2(\hat{\gamma})$)

$$\begin{cases} \gamma_0 \leq \gamma''_0, & \eta \leq f_1(\hat{\gamma}), \\ \gamma_0 > \gamma''_0, & \eta > f_1(\hat{\gamma}). \end{cases} \quad (62)$$

Thus, we can further draw the conclusion that

$$\begin{cases} r(\gamma) \text{ is convex-concave,} & \eta \geq \frac{(\hat{\gamma} + 1)\ln(\hat{\gamma} + 1)}{\sqrt{\hat{\gamma}^2 + 2\hat{\gamma}}}, \\ r(\gamma) \text{ is concave,} & \eta > \frac{(\hat{\gamma} + 1)\ln(\hat{\gamma} + 1)}{\sqrt{\hat{\gamma}^2 + 2\hat{\gamma}}}. \end{cases} \blacksquare$$

APPENDIX B
PROOF OF **Theorem 2**

For simplicity, we rewrite the cycle rate and the rate-cost function as the functions of SNR, i.e., $R(\gamma)$ and $L(\gamma)$. In addition, a new function is introduced as follows

$$\Omega(\gamma) = R(\gamma) - \log_2 |\det \mathbf{A}|. \quad (63)$$

To figure out the convexity of $L(\gamma)$, we calculate its second derivative

$$\begin{aligned} \nabla^2 L(\gamma) &= \frac{2^{\frac{2}{m}\Omega(\gamma)+1} |\det \mathbf{N}\mathbf{M}|^{\frac{1}{m}}}{\log_2 e (2^{\frac{2}{m}\Omega(\gamma)} - 1)^2} \times \\ &\quad \left[\frac{2}{m \log_2 e} \left(\frac{2^{\frac{2}{m}\Omega(\gamma)} + 1}{2^{\frac{2}{m}\Omega(\gamma)} - 1} \right) [\nabla \Omega(\gamma)]^2 - \nabla^2 \Omega(\gamma) \right], \end{aligned} \quad (64)$$

where $\nabla \Omega(\gamma)$ and $\nabla^2 \Omega(\gamma)$ are given by

$$\nabla \Omega(\gamma) = \log_2 e \left(\frac{n}{\gamma + 1} - \frac{\sqrt{n} Q^{-1}(\epsilon)}{(\gamma + 1)^2 \sqrt{\gamma^2 + 2\gamma}} \right), \quad (65)$$

$$\begin{aligned} \nabla^2 \Omega(\gamma) &= \log_2 e \left(-\frac{n}{(\gamma + 1)^2} + \right. \\ &\quad \left. \sqrt{n} Q^{-1}(\epsilon) \frac{(\gamma + 1)^2 + 2(\gamma^2 + 2\gamma)}{(\gamma + 1)^3 (\gamma^2 + 2\gamma)^{\frac{3}{2}}} \right). \end{aligned} \quad (66)$$

Accordingly, we define two functions as follows

$$f(m, \gamma) \triangleq \frac{2}{m \log_2 e} \left(\frac{2^{\frac{2}{m}\Omega(\gamma)} + 1}{2^{\frac{2}{m}\Omega(\gamma)} - 1} \right) [\nabla \Omega(\gamma)]^2 - \nabla^2 \Omega(\gamma), \quad (67)$$

$$g(m, \Omega) \triangleq \frac{2}{m \log_2 e} \left(\frac{2^{\frac{2}{m}\Omega} + 1}{2^{\frac{2}{m}\Omega} - 1} \right). \quad (68)$$

We first prove that $g(m, \Omega)$ is monotonically decreasing with m . Its partial derivative of m is given by

$$\frac{\partial g(m, \Omega)}{\partial m} = \frac{2}{\log_2(e) m^2 (2^{\frac{2\Omega}{m}} - 1)^2} \left[\frac{\Omega 2^{\frac{2\Omega}{m}+2}}{m \log_2 e} - 2^{\frac{4\Omega}{m}} + 1 \right]. \quad (69)$$

The sign of $\frac{\partial g(m, \Omega)}{\partial m}$ is determined by term $\left[\frac{\Omega 2^{\frac{2\Omega}{m}+2}}{m \log_2 e} - 2^{\frac{4\Omega}{m}} + 1 \right]$. It is obvious that

$$\frac{\Omega 2^{\frac{2\Omega}{m}+2}}{m \log_2 e} - 2^{\frac{4\Omega}{m}} + 1|_{\Omega=0} = 0. \quad (70)$$

In addition, we calculate the partial derivative of the above expression of Ω . The expression is given by

$$\frac{2^{\frac{2\Omega}{m}+2}}{m \log_2 e} \left(\frac{2\Omega}{m \log_2 e} + 1 - 2^{\frac{2\Omega}{m}} \right). \quad (71)$$

Since $e^x \geq x + 1$, we could find that $\frac{2\Omega}{m \log_2 e} + 1 - 2^{\frac{2\Omega}{m}} \leq 0$. Based on (70), it is easy to draw that

$$\frac{\partial g(m, \Omega)}{\partial m} |_{\Omega \geq 0} \leq 0. \quad (72)$$

Therefore, $g(m, \Omega)$ is monotonically decreasing with m . The minimal value of $f(m, \gamma)$ is obtained when m goes to infinity. If we could prove $\lim_{m \rightarrow +\infty} f(m, \gamma) \geq 0$, the non-negativity of $\nabla^2 L(\gamma)$ can be proven.

In the following, we consider the limit case of $m \rightarrow +\infty$. In this case, the index number $\frac{2\Omega}{m}$ in $g(m, \Omega)$ can be arbitrarily

small. To facilitate the simplification, we assume $\frac{2\Omega}{m} \leq 1$. Then, it is easy to have the following scaling

$$\frac{2\Omega}{m} \leq 1 \Rightarrow 2^{\frac{2}{m}\Omega} - 1 \leq \frac{4\Omega}{m \log_2 e}. \quad (73)$$

On this basis, we can further scale $g(m, \Omega)$ as follows

$$\begin{aligned} \lim_{m \rightarrow +\infty} g(m, \Omega) &= \lim_{m \rightarrow +\infty} \frac{2}{m \log_2 e} \left(1 + \frac{2}{2^{\frac{2}{m}\Omega} - 1} \right) \\ &\geq \frac{4}{m \log_2 e (2^{\frac{2}{m}\Omega} - 1)} \geq \frac{4}{m \log_2 e \left(\frac{4\Omega}{m \log_2 e} \right)} = \frac{1}{\Omega} \end{aligned} \quad (74)$$

Moving forward, by substituting (74) into (67), we have

$$\lim_{m \rightarrow +\infty} f(m, \gamma) \geq \frac{1}{\Omega(\gamma)} [\nabla \Omega(\gamma)]^2 - \nabla^2 \Omega(\gamma). \quad (75)$$

Furthermore, $\Omega(\gamma)$ can be scaled such that

$$\Omega(\gamma) \leq n \log_2(\gamma + 1) \leq n\gamma \log_2 e. \quad (76)$$

In addition, as we mentioned after (21), the definition domain of $L(\gamma)$ is determined by the stable condition

$$\begin{aligned} R(\gamma) - \log_2 |\det \mathbf{A}| &\geq 0 \\ &\Rightarrow R(\gamma) \geq 0 \\ &\Rightarrow Q^{-1}(\epsilon) < \frac{\sqrt{n} \log_2(\gamma + 1)}{\log_2 e \sqrt{1 - \frac{1}{(\gamma+1)^2}}}. \end{aligned} \quad (77)$$

By substituting $Q^{-1}(\epsilon)$ with the right side of (77), we could derive the following inequality of $\nabla \Omega(\gamma)$ shown in (65) and $\nabla^2 \Omega(\gamma)$ shown in (66)

$$\begin{aligned} \nabla \Omega(\gamma) &\geq n \log_2 e \left(\frac{1}{\gamma + 1} - \frac{\log_2(\gamma + 1)}{\log_2 e (\gamma + 1) (\gamma^2 + 2\gamma)} \right) \\ &\geq n \log_2 e \left(\frac{1}{\gamma + 1} - \frac{1}{(\gamma + 1)(\gamma + 2)} \right), \end{aligned} \quad (78)$$

$$\begin{aligned} \nabla^2 \Omega(\gamma) &\leq n \log_2 e \left(-\frac{1}{(\gamma + 1)^2} + \right. \\ &\quad \left. \frac{\log_2(\gamma + 1)}{\log_2 e} * \frac{(\gamma + 1)^2 + 2(\gamma^2 + 2\gamma)}{(\gamma + 1)^2 (\gamma^2 + 2\gamma)^2} \right) \\ &\leq n \log_2 e \left(-\frac{1}{(\gamma + 1)^2} + \frac{(\gamma + 1)^2 + 2(\gamma^2 + 2\gamma)}{\gamma(\gamma + 1)^2 (\gamma + 2)^2} \right). \end{aligned} \quad (79)$$

By substituting (76), (78) and (79) into (75), we have that

$$\begin{aligned} \lim_{m \rightarrow +\infty} f(m, \gamma) &\geq \\ &\frac{1}{n\gamma \log_2 e} \left(n \log_2 e \left(\frac{1}{\gamma + 1} - \frac{1}{(\gamma + 1)(\gamma + 2)} \right) \right)^2 - \\ &n \log_2 e \left(-\frac{1}{(\gamma + 1)^2} + \frac{(\gamma + 1)^2 + 2(\gamma^2 + 2\gamma)}{\gamma(\gamma + 1)^2 (\gamma + 2)^2} \right) \\ &= \frac{n\gamma \log_2 e}{(\gamma + 1)^2 (\gamma + 2)} \geq 0. \end{aligned} \quad (80)$$

Therefore, for any m , we have that

$$\nabla^2 L(\gamma) \geq \lim_{m \rightarrow +\infty} f(m, \gamma) \geq 0. \quad (81)$$

The convexity of $L(\gamma)$ is thus proven. ■

REFERENCES

- [1] Y. Zheng, "Mars exploration in 2020," *The innovation*, [Online], Available: [https://www.cell.com/the-innovation/pdf/S2666-6758\(20\)30036-9.pdf](https://www.cell.com/the-innovation/pdf/S2666-6758(20)30036-9.pdf).
- [2] "Zhurong(rover)," *Wikipedia*, [Online], Available: [https://en.wikipedia.org/wiki/Zhurong_\(rover\)](https://en.wikipedia.org/wiki/Zhurong_(rover)).
- [3] R. Xie, "Tianwen · Exploring Mars — Successfully landed on Mars! Tianwen-1 withstood the test of 9 minutes of terror," [Online], Available: https://www.thepaper.cn/newsDetail_forward_12690263.
- [4] R. McCormick *et al.*, "Development of miniature robotic manipulators to enable SmallSat clusters," in *Proc. 2017 IEEE Aerosp. Conf.*, Big Sky, MT, USA, 2017, pp. 1-15.
- [5] F. Davarian *et al.*, "Improving small satellite communications and tracking in deep space—A review of the existing systems and technologies with recommendations for improvement. Part III: The deep space network," *IEEE Aerosp. Electron. Syst. Mag.*, vol. 35, no. 8, pp. 4-13, Aug. 2020.
- [6] J. Baillieul and P. J. Antsaklis, "Control and communication challenges in networked real-time systems," in *Proc. IEEE*, vol. 95, no. 1, pp. 9-28, Jan. 2007.
- [7] R. A. Gupta and M. -Y. Chow, "Networked control system: Overview and research trends," *IEEE Trans. Ind. Electron.*, vol. 57, no. 7, pp. 2527-2535, Jul. 2010.
- [8] L. Zhang, H. Gao, and O. Kaynak, "Network-induced constraints in networked control systems—A survey," *IEEE Trans. Ind. Electron.*, vol. 9, no. 1, pp. 403-416, Feb. 2013.
- [9] T. Ha, J. Oh, D. Lee, J. Lee, Y. Jeon, and S. Cho, "Reinforcement learning-based resource allocation for streaming in a multi-modal deep space network," in *Proc. 2021 Int. Conf. Info. Commun. Tech. Convergence (ICTC)*, Jeju Island, Korea, 2021, pp. 201-206.
- [10] G. Xu and Q. Zhang, "Mixed RF/FSO deep space communication system under solar scintillation effect," *IEEE Trans. Aerosp. Electron. Sys.*, vol. 57, no. 5, pp. 3237-3251, Oct. 2021.
- [11] L. Yang *et al.*, "Resource consumption of a hybrid bundle retransmission approach on deep-space communication channels," *IEEE Aerosp. Electron. Sys. Mag.*, vol. 36, no. 11, pp. 34-43, 1 Nov. 2021.
- [12] F. De Rango and M. Tropea, "DTN architecture with resource-aware rate adaptation for multiple bundle transmission in interplanetary networks," *IEEE Access*, vol. 10, pp. 47219-47234, Apr. 2022.
- [13] P. Wan, and Y. Zhan, "A structured solar system satellite relay constellation network topology design for Earth-Mars deep space communications," *Int. J. Satell. Commun. Netw.*, vol.37, no. 3, pp. 292-313, Jan. 2019.
- [14] S. Tatikonda and S. Mitter, "Control under communication constraints," *IEEE Trans. Autom. Control*, vol. 49, no. 7, pp. 1056-1068, Jul. 2004.
- [15] B. G. N. Nair, F. Fagnani, S. Zampieri, and R. J. Evans, "Feedback control under data rate constraints: An overview," in *Proc. IEEE*, vol. 95, no. 1, pp. 108-137, Jan. 2007.
- [16] G. N. Nair, R. J. Evans, I. M. Y. Mareels, and W. Moran, "Topological feedback entropy and nonlinear stabilization," *IEEE Trans. Autom. Control*, vol. 49, no. 9, pp. 1585-1597, Sep. 2004.
- [17] V. Kostina and B. Hassibi, "Rate-cost tradeoffs in control," *IEEE Trans. Autom. Control*, vol. 64, no. 11, pp. 4525-4540, Nov. 2019.
- [18] M. S. Branicky, S. M. Phillips and Wei Zhang, "Stability of networked control systems: Explicit analysis of delay," in *Proc. 2000 American Control Conf.*, Chicago, IL, USA, 2000.
- [19] L. Zhang, C. Wang, and Y. Chen, "Stability and stabilization of a class of multimode linear discrete-time systems with polytopic uncertainties," *IEEE Trans. Ind. Electron.*, vol. 56, no. 9, pp. 3684-3692, Sep. 2009.
- [20] H. Lin and P. J. Antsaklis, "Persistent disturbance attenuation properties for networked control systems," in *Proc. 43rd Conf. Decis. Control*, Dec. 2004, vol. 1, pp. 953-958.
- [21] L. Lyu, C. Chen, S. Zhu, N. Cheng, B. Yang, and X. Guan, "Control performance aware cooperative transmission in multiloop wireless control systems for industrial IoT applications," *IEEE Internet Things J.*, vol. 5, no. 5, pp. 3954-3966, Oct. 2018.
- [22] A. M. Girgis, J. Park, C. -F. Liu, and M. Bennis, "Predictive control and communication co-design: A Gaussian process regression approach," in *Proc. 2020 IEEE 21st SPAWC*, 2020, pp. 1-5.
- [23] H. Yang, K. Zhang, K. Zheng, and Y. Qian, "Leveraging linear quadratic regulator cost and energy consumption for ultrareliable and low latency IoT control systems," *IEEE Internet Things J.*, vol. 7, no. 9, pp. 8356-8371, Sep. 2020.
- [24] C. Lei, W. Feng, J. Wang, S. Jin, and N. Ge, "Control-oriented power allocation for integrated satellite-UAV networks," *IEEE Wireless Commun. Lett.*, vol. 12, no. 5, pp. 883-887, May 2023.
- [25] B. Chang, G. Zhao, L. Zhang, M. A. Imran, Z. Chen, and L. Li, "Dynamic communication QoS design for real-time wireless control systems," *IEEE Sensors J.*, vol. 20, no. 6, pp. 3005-3015, Mar. 2020.
- [26] M. Eisen, M. M. Rashid, K. Gatsis, D. Cavalcanti, N. Himayat, and A. Ribeiro, "Control aware radio resource allocation in low latency wireless control systems," *IEEE Internet Things J.*, vol. 6, no. 5, pp. 7878-7890, Oct. 2019.
- [27] X. Pan, Y. Zhan, P. Wan, *et al.* "Review of channel models for deep space communications," *Sci. China Inf. Sci.*, vol. 61, pp. 1-12, Jan. 2018.
- [28] "Study on New Radio (NR) to support non-terrestrial networks". *3GPP TR 38.811 v15.4.0*, Sep. 2020.
- [29] J. Tang, D. Bian, G. Li, J. Hu, and J. Cheng, "Resource allocation for LEO beam-hopping satellites in a spectrum sharing scenario," *IEEE Access*, vol. 9, pp. 56468-56478, 2021.
- [30] Y. Polyanskiy, H. V. Poor, and S. Verdú, "Channel coding rate in the finite blocklength regime," *IEEE Trans. Inf. Theory*, vol. 56, no. 5, pp. 2307-2359, May 2010.
- [31] Yang W, Durisi G, and Koch T, "Quasi-static multiple-antenna fading channels at finite blocklength", *IEEE Trans. Inf. Theory*, vol. 60, no. 7, pp. 4232-4264, Jul. 2014.
- [32] C. Sun, C. She, C. Yang, T. Q. S. Quek, Y. Li, and B. Vucetic, "Optimizing resource allocation in the short blocklength regime for ultra-reliable and low-latency communications," *IEEE Trans. Wireless Commun.*, vol. 18, no. 1, pp. 402-415, Jan. 2019.
- [33] T. M. Cover and J. A. Thomas, *Elements of Information Theory*, Hoboken, NJ, USA: Wiley, 2006.